Title

Calcium Ion Bridging of Aqueous Carboxylates onto Silica: Implications for Low-Salinity Waterflooding

Journal

Energy & Fuels, 33(1)

ISSN

0887-0624

Authors

Hu, Xiaozhen
Yutkin, Maxim P
Hassan, Saleh
et al.

Publication Date

2019-01-17

DOI

10.1021/acs.energyfuels.8b03366

Peer reviewed

Calcium Ion Bridging of Aqueous Carboxylates onto Silica: Implications for Low-Salinity Waterflooding

Xiaozhen Hu,[†,§] Maxim P. Yutkin,[‡] Saleh Hassan,[‡] Jiangtao Wu,[§] J. M. Prausnitz,[†] and C. J. Radke*[,†,‡]

[†] Department of Chemical and Biomolecular Engineering, University of California, Berkeley, Berkeley, California 94720, United States [‡] Ali I. Al-Naimi Petroleum Engineering Research Center (ANPERC), Physical Sciences and Engineering Division, King Abdullah University of Science and Technology (KAUST), Thuwal 23955-6900, Kingdom of Saudi Arabia [§] Key Laboratory of Thermo-Fluid Science and Engineering of Ministry of Education, Xi'an Jiaotong University, Xi'an, Shaanxi 710049, People's Republic of China

*Telephone: 510-642-5204. Fax: 510-642-4778. E-mail: radke@berkeley.edu

Abstract

Release of crude oil from reservoir rock by low-salinity waterflooding is thought to occur by decreasing the advancing crude oil/brine/rock water contact angle to depin three-phase contact lines (i.e., by increasing reservoir water wettability). Crude oil likely adheres locally to reservoir rock asperities by deposition of asphaltene agglomerates formed at the crude oil/brine interface, following collapse of protective water films. One mechanism proposed for asphaltene adhesion and subsequent release is ion bridging of asphaltenic carboxylate groups protruding through molecularly thin water layers to calcium-occupied rock surface exchange sites, the so-called multicomponent ion exchange mechanism. To our knowledge, however, no experimental evidence directly establishes divalent cation bridging of aqueous carboxylates to anionic mineral surfaces. Using a quartz crystal microbalance with dissipation, we measure adsorption of aqueous carboxylates (benzoate, pentanoate, and hexanoate) onto silica, with and without calcium ion present at near-neutral pH. We find little to no adsorption on a silica surface to within the detection limit of our measurement (±1 Hz, 0.18 mg/m2). Modeling of the silica surface chemistry, using classical ion-complexing triple-layer formalism, reveals that less than 10% of surface-hydroxylated sites actually ionize at pH 7. Of these, not all bind calcium ions. Accordingly, the calcium ion surface density is insufficient to reverse the negative surface charge of silica or to promote significant ion bridging of aqueous carboxylates. In so far as aqueous-soluble carboxylic acids mimic those incorporated in crude oil asphaltenes, we conclude that calcium ion bridging alone does not adhere asphaltenes to silica surfaces.

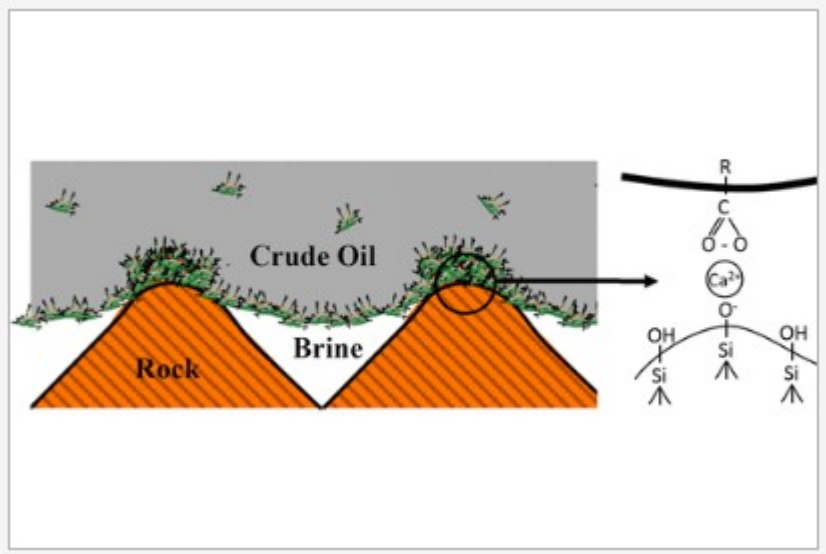

1. Introduction

Waterflooding to recover reservoir crude oil is widespread. Typically, floodwater is acquired from nearby available sources. Minimal attention is paid to the detailed chemistry of the water, because enhanced recovery by waterflooding is considered a physical process. However, the pioneering work of Morrow and co-workers(1−7) established that simple lowering of brine salinity could improve oil recovery in sandstones.

There is agreement that incremental oil from low-salinity waterflooding (LSW) relies on a shift of reservoir wettability toward water-wet. (8)Figure 1 envisions how crude oil likely adheres to rough reservoir rock. (8−12) The crude oil/brine/rock (COBR) configuration pictured in Figure 1 is coined mixed-wet because water occupies the crevises of the rock surfaces and oil occupies the remaining voidage, all within the same local pore space. (13) Mixed wetting is the result of aqueous-insoluble asphaltenes in the crude oil that aggregate at the oil/water interface.(9,14) As oil invades into an initially brine-occupied reservoir rock, water recedes into pore corners and roughness. Water films separating the rock from crude oil(15) rupture near roughness asperity cusps, bringing interfacial asphaltene agglomerates into direct molecular contact with mineral surfaces.(8,9,16,17) Near roughness apexes, the mineral surface is oil-wet, while rock surfaces remain water-wet in roughness crevices.

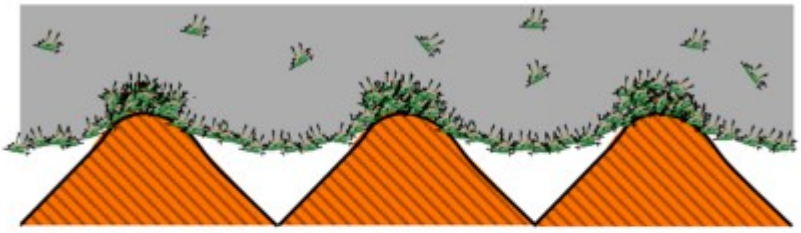

Figure 1. Dalmation or speckled mixed wetting of rough reservoir rock. White indicates water; gray is crude oil; and rock is red-striped. Asphaltene molecules are shown in the oil, agglomerated at the oil/water interface, and attached to rock apexes. Oil/water/brine interfaces are pinned near the rock crests because of asphaltene deposition.

Rock-attached asphaltenes pin the three-phase contact lines, preventing oil mobilization.(14) In analogy to the “roll up” cleaning mechanism in detergency,(18) oil mobilization requires depinning of the contact lines by reducing the water contact angle between the oil and rock to the advancing value.(19) However, the molecular mechanism initiating contact line depinning is not settled.(10−12,20) Numerous mechanisms are proposed, including clay swelling and fines migration, pH increase and surfactant generation, electrical double-layer expansion, and multicomponent ion exchange (MIE), among others.(12,21) Yutkin et al.(21) propose that MIE is a viable oil release mechanism, although direct proof lags.(12)

Lager et al.(22) originally proposed MIE as a possible oil recovery mechanism in LSW. In MIE, polar components in asphaltenes affixed to the oil/water interface attach to charged rock surfaces through aqueous metal–ion complexes. Attachment of asphaltenes to rock surfaces occurs only when protective water films between the oil and rock rupture, permitting direct molecular contact with mineral surface exchange sites.
(8,9,14,23) Asphaltenes contain several candidate ion exchange groups, for example, carboxyl, pyridine, and pyrrole.(24,25) We focus on carboxylated side chains because they are end-terminated and anionic at typical reservoir pH values above about 7, whereas heterocyclic amines are less accessible and have acidic pK_a values near 5.(26,27) Once water films rupture, divalent metal ion complexing of asphaltenic carboxylated side groups can adhere the crude oil to negative mineral surfaces through divalent cation ion bridging(22,28) or

$$\begin{aligned} &\equiv S^- + M^{2+} \rightleftharpoons \equiv S\,M^{2+} \\ &\equiv S\,M^{2+} + RCOO^- \rightleftharpoons \equiv S\,M^{2+}(\,COOCR) \end{aligned} \quad (1)$$

where $\equiv S^-$ is a mineral anionic surface exchange site, M^{2+} is an aqueous divalent cation, such as calcium or magnesium, and $RCOO^-$ designates an carboxylated asphaltenic side group. Accordingly, carboxylate moieties bridged to a mineral surface act as molecular “stickers”. Figure 2 provides a schematic of the bridging mechanism. As a result of electrostatic repulsion,

anionic surfactants and polymers commonly do not adsorb onto negatively charged mineral surfaces. Multivalent cation bridging, however, provides a mechanism to adsorb anionic aqueous species to negative solid surfaces. (29−32)

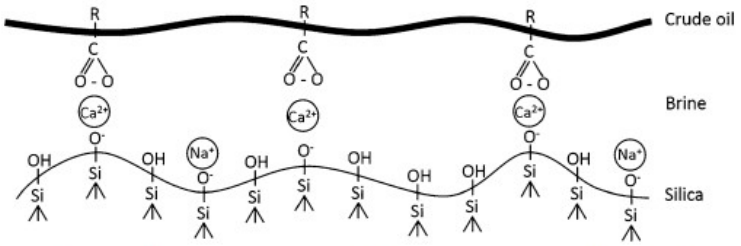

Figure 2. Schematic of dangling asphaltene carboxylate groups at the COBR interface ion complex through calcium ion binding to anionic surface hydroxide sites on a silica surface. Calcium ion complexes serve as asphaltene stickers (not drawn to scale).

According to eq 1, release of mineral-adhered asphaltene side groups can occur by reducing the aqueous divalent cation concentration during LSW. Alternatively, the addition of solution anions that more strongly ion bridge can also release carboxylate side groups or $\equiv S^-M^{2+}(^-OOCR) + X^- \rightleftarrows \equiv S^-M^{2+}X^- + RCOO^-$ (2)where X^- is an aqueous anion with high bridging affinity compared to the carboxylate anion. In eq 2, low salinity is not required for oil mobilization.

Although MIE is appealing, divalent cation ion bridging of anionic aqueous solutes to negative mineral surfaces has not been extensively studied. Using a quartz crystal microbalance with dissipation (QCMD), Wang et al. (30) reported that adsorption of sodium hexanoate on quartz is significantly enhanced by the presence of calcium ions in solution. Sposito and co-workers(29,32) suggest calcium ion bridging of humic acids to montmorillonite in soils. Indirect evidence for calcium ion bridging onto silica is available from contact angle measurement,(33,34) specular neutron reflection,(31) and ζ-potential measurement.(35) Spildo et al.(36) reported the adsorption of sodium benzoate in aqueous solution on several different silica surfaces and interpreted the adsorption as “sodium ion bridging”. Zaman et al.,(37) however, found no adsorption of low-molecular-weight sodium poly(acrylic acid) on silica particles.

We mimic possible sticking of carboxylate pendant chains emanating from asphaltene agglomerates to an anionic mineral surface by studying adsorption of soluble aqueous acids (benzoate, pentanoate, and hexanoate) onto silica using QCMD with and without calcium present. Silica was the chosen mineral surface because it is the major mineral in sandstone reservoirs and because QCMD sensors are readily available. Aqueous solution pH was near-neutral, where the soluble organic acids are deprotonated as are the surface hydroxyl groups of silica.(38) The classical triple-layer ionogenic surface chemistry model(39−41) elucidates our results.

2. Materials and Methods

2.1. Chemicals

We propose that water-soluble carboxylic anions capture the essential behavior of pendant carboxylated groups extending from oil/water interfacial asphaltene agglomerates. Although asphaltene is water-insoluble, its surface carboxyl groups at the oil/water interface should adsorb similarly to those of soluble carboxylic anions. Sodium benzoate (NaBen, 99%, Fluka), sodium hexanoate (NaHex, 99%, Sigma-Aldrich), and calcium pentanoate [$Ca(Pen)_2$] were used for this purpose. $Ca(Pen)_2$ was prepared by mixing calcium hydroxide (98%, ACROS) with pentanoic acid (HPen, 99%, ACROS). Cetyltrimethylammonium bromide (CTAB, 98%, Fluka) and tetraethylene glycol monodecyl ether ($C_{10}E_4$, 97%, Fluka) surfactants were chosen as cationic and non-ionic surfactants, respectively, to validate the performance of the QCMD apparatus. Sodium chloride (NaCl, 99.9%, certified ACS, Fisher Chemicals) and calcium chloride dihydrate ($CaCl_2 \cdot 2H_2O$, 99.9%, certified ACS, Fisher Chemicals) were used to provide mono- and divalent cations. All chemicals were used as received; no further purification was made. Distilled/deionized water was from a Milli-Q cartridge system (Synergy, EMD Millipore Corporation), giving resistivity greater than 18.2 MΩ cm at 25 °C.

2.2. QCMD Procedures

A QCMD E4 (Biolin Scientific, Gothenburg, Sweden) was used to measure aqueous carboxylate adsorption. QCMD is convenient for adsorption studies, providing not only adsorption amounts but also adsorption and desorption kinetics.(42) Silica sensors (QXS 303) were used as the adsorbent. To minimize signal drift, each sensor was reused for less than 5 times. Nevertheless, some variation was observed, especially for “older” sensors. Pristine and previously used silica sensors were cleaned by the following procedures. First, the sensors were rinsed with Milli-Q water, followed by gentle blow-drying with filtered dry nitrogen. Dry sensors were then plasma-cleaned (Harrick Plasma Cleaner, 110 V, PDC-32G, medium intensity) for 10 min. After plasma cleaning, sensors were immediately transferred into the flow modules (QFM 401) and aligned to the desired position. The temperature was constant at 25 °C. Milli-Q water was flushed through the cells with a peristaltic pump (ISM935C, Ismatec) at 100 μL/min. Resonant frequencies and dissipation of the first, third, fifth, seventh, and ninth overtones were recorded simultaneously. Flushing was continuous for 1–2 h until any frequency shift at each overtone was smaller than 0.2 Hz/h. Subsequent to a stable reference signal, a baseline solution (pure water, NaCl or $CaCl_2$ solutions listed in Table1) was injected for 10–15 min, followed by continuous injection of the acid sample solution. After the adsorption kinetic measurement (typically 20–30 min), inlet carboxylate solution was changed back to baseline solution to assess possible irreversible adsorption. Throughout the procedure, frequency shift and dissipation change were recorded. Each experiment was repeated 2 or 4 times by using 2 or 4 individual sensors. After each measurement, Milli-Q water was flushed at 200 μL/min for 1 h to rinse the entire system. Similar experiments were performed independently with a QSense Pro QCMD instrument (Biolin

Scientific, Gothenburg, Sweden) located at KAUST (Thuwal, Kingdom of Saudi Arabia).

Table 1. QCMD Results for Carboxylates (Fifth Overtone Only)[a]

baseline	sample	$\Delta f_{5,exp}/5$ (Hz)	$\Delta D_{5,exp}$ ($\times 10^6$)	$\Delta f_{5,corr}/5$ (Hz)[b]	$\Delta f_{5,corr}/5$ (Hz)[c]	Γ (μmol/m^2)[d]	Γ (μmol/m^2)[d]
water	80 mM NaBen	−6.4 ± 0.3	2.7 ± 0.2	0.8 ± 0.3	0.3 ± 0.3	0	0
100 mM $CaCl_2$	100 mM $CaCl_2$	−6.9 ± 0.4	2.6 ± 0.4	0.3 ± 0.4	0.5 ± 0.4	0	0
	80 mM NaBen						
water	100 mM NaBen	−7.4 ± 0.2	3.1 ± 0.2	0.9 ± 0.2	0.3 ± 0.2	0	0
50 mM NaCl	50 mM NaCl	−8.2 ± 0.4	3.3 ± 0.1	0.1 ± 0.4	0.0 ± 0.4	0	0
	100 mM NaBen						
50 mM $CaCl_2$	50 mM $CaCl_2$	−9.7 ± 0.8	3.6 ± 0.2	−1.4 ± 0.8	−0.8 ± 0.8	2.1 ± 1.2	1.2 ± 1.2
	100 mM NaBen						
water	100 mM NaHex	−10.5 ± 0.5	4.2 ± 0.2	−0.1 ± 0.5	−0.1 ± 0.5	0.2 ± 0.8	0.2 ± 0.8
50 mM NaCl	50 mM NaCl	−11.2 ± 0.1	4.3 ± 0.4	−0.8 ± 0.1	−0.6 ± 0.1	1.2 ± 0.2	0.9 ± 0.2
	100 mM NaHex						
50 mM $CaCl_2$	50 mM $CaCl_2$	−11.9 ± 1.2	4.6 ± 0.3	−1.5 ± 1.2	−0.5 ± 1.2	2.3 ± 1.9	0.8 ± 1.8
	100 mM NaHex						
10 mM NaCl	10 mM NaHex	−0.9 ± 0.7	0.5 ± 0.1	0.3 ± 0.7	0.3 ± 0.7	0	0
20 mM $CaCl_2$	20 mM $CaCl_2$	−3.0 ± 0.6	0.6 ± 0.1	−1.7 ± 0.6	−1.5 ± 0.6	2.6 ± 0.9	2.3 ± 0.9
	10 mM NaHex						
350 mM $CaCl_2$	200 mM $Ca(Pen)_2$	−26.2 ± 0.4	10.2 ± 0.1		−1.0 ± 0.4		1.8 ± 0.7

[a]Uncertainty was calculated according to measurement repeatability. For carboxylate samples, the pH ranges from 7 to 8.5. [b]Frequency shift was corrected according to eq 8. [c]Frequency shift was corrected according to eq 10. [d]Adsorption amount was calculated by the Sauerbrey equation (eq 3) according to columns 5 and 6 and converted to mole units after division by the molecular weight of anions. Zero adsorption is listed for positive-corrected frequency shifts.

2.3. QCMD Interpretation

Increasing the mass of the oscillating crystal by solute adsorption lowers the oscillation frequency and leads to the classical Sauerbrey relation(43)

$$\hat{\Gamma} = -C\frac{(f - f^*)}{n} = -C\frac{\Delta f}{n} \quad (3)$$

where $\hat{\Gamma}$ is the solute-adsorbed mass density (mass/area), commonly written as Δm,(44)f^* is the bare crystal frequency (5 MHz), f is the measured frequency with adsorbed mass, n is the overtone number (1, 3, 5, etc.), and C (=17.7 ng cm^{-2} Hz^{-1} for 5 MHz AT-cut quartz crystal) is an apparatus constant (see below). Thus, the adsorbed amount is directly available from QCMD with no prior calibration.

When liquid-soluble species adsorb, however, crystal oscillation also oscillates the covering liquid, altering both frequency and dissipation. Equation 3 is no longer valid and must be modified. Figure 3 pictures solute molecules adsorbed to the substrate crystal and dissolved in an overlying Newtonian liquid solution of bulk density ρ and viscosity η. The characteristic distance over which the liquid oscillates is δ [=$(2\eta/\rho\omega)^{1/2}$], where ω is the crystal angular frequency.(45) For frequencies near $f = \omega/2\pi$ = 5 MHz, the penetration distance in pure water is about 0.25 μm at 25 °C, a distance considerably larger than that of molecular-adsorbed layers.

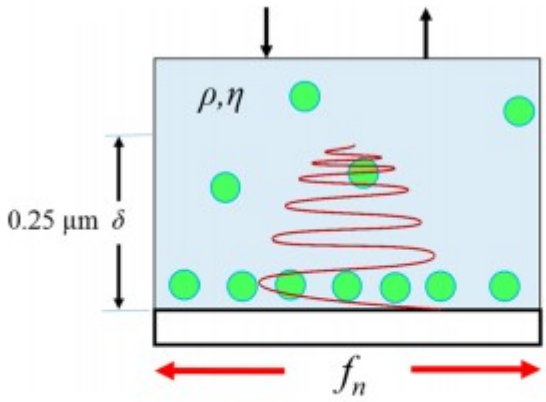

Figure 3. Liquid solute adsorption on the QCMD substrate. The solute is pictured as a sphere. δ labels the thickness over which the quartz plate oscillation is felt in the overlayer solution (curved lines), at approximately 0.25 μm for water.

Solute molecules are affixed to the substrate solid and do not flow. The adsorbed layer is modeled as purely elastic and homogeneous of thickness h_L and density ρ_L. Under these approximations, Voinova et al. (46) established that

$$\frac{\Delta f_n}{n} = \frac{(f_n - f^*)}{n} = -\frac{f^*}{h_q \rho_q} h_L \rho_L + \frac{1}{n^{3/2}} \frac{df^*/\pi}{2h_q \rho_q} \sqrt{\eta_L \rho_L} + O(k_L h_L)^2 \quad (4)$$

where the product $h_L\rho_L$ in the homogeneous adsorbed layer model is solute-adsorbed mass density; i.e., $\rho_L h_L \equiv \Gamma$. Hence, the instrument constant C in eq 3 is defined by $C \equiv h_q\rho_q/f^*$, where h_q is the thickness of the quartz crystal and ρ_q is its mass density. k_L in eq 4 is the wavenumber of the adsorbed layer defined by $k_L \equiv (\rho_L\omega^2/\mu_L)^{1/2}$, where μ_L is the shear elastic modulus of the adsorbed layer, presumed constant, independent of the layer thickness. The last term contributes to second-order in film thickness and is neglected in this work. With these definitions, eq 4 transforms to

$$\frac{\Delta f_n}{n} = -\frac{1}{C}\Gamma - \frac{f^*}{n^{3/2}} \sqrt{\eta_L \rho_L} \quad (5)$$

where the factor $\beta \equiv (f^*/\pi)^{1/2}/2h_q\rho_q$ is a second instrument constant. The first term on the right of eq 5 is the celebrated Sauerbrey relation of eq 1. Adsorption reduces the frequency of the vibrating crystal. This term is independent of the particular overtone number. The second term corrects for oscillation of the overlying liquid solution and scales inversely with the square root of the overtone number. For non-adsorbing liquid solutions, QCMD frequency (and dissipation) shifts provide a sensitive means to measure solution viscosity.(47,48)

Similarly, Voinova et al.(46) derived the corresponding change in dissipation for an elastic-adsorbed layer covered by a liquid solution as

 (6)

Dissipation is dimensionless and positive relative to the crystal oscillating in air. It is attributed to viscous dissipation in the liquid overlayer plus that given by a second term inversely proportional to the elastic modulus of the adsorbed layer. For a thin adsorbed film, the second and third terms on the right of eq 6 are negligible; dissipation is due only to the liquid overlayer or

 (7)

There is no dissipation contribution from a purely elastic adsorbed layer.

In our experiments, frequency and dissipation shifts are measured relative to a baseline composition, typically salt solutions devoid of adsorbing solute, or $\Delta f_n = f - f_o$ and $\Delta D_n = D - D_o$. Hence, the viscosity–density terms in eqs 5 and 7, respectively, change to

 (8)

And

 (9)

where the o subscript indicates a baseline solution. For simple, non-adsorbing aqueous electrolytes, Appendix A of the Supporting Information confirms the viscosity–density theory correction in eqs 8 and 9. A linear dependence of $\Delta f_n/n$ and ΔD_n upon the difference in the square root of density times viscosity emerges experimentally as exemplified in Figures A.1 and A.2 of the Supporting Information using no adjustable constants. Thus, eqs 8 and 9 provide a framework for interpreting liquid solution adsorption results. Correction for viscosity and density of the liquid solution overlayer is available from separate measurements of solution density and viscosity and/or eq 9 and measurement of the corresponding dissipation shift

 (10)

We use both viscosity–density correction methods.

3. Results

3.1. QCMD Validation

To assess the adsorption performance of QCMD for liquid solutions, we measured the adsorption of CTAB (cationic) and $C_{10}E_4$ (nonionic) aqueous surfactants on the silica surface at their critical micelle concentration (cmc) (i.e., 1 mM for CTAB(49) and 0.86 mM for $C_{10}E_4$(50)). Solutions were slightly acidic at pH 6 as a result of contact with ambient air. Figures B.1 and B.2 in Appendix B of the Supporting Information present the

frequency (black) and dissipation (red) kinetics. Because data for different overtones follow eqs 8 and 9, only the fifth overtone is presented here. Dissipation slightly increases by about 0.1–0.2 unit. This result means that the viscosity–density correction relative to pure water is negligible at the studied low bulk concentrations. We, thus, interpret the reported sharp frequency declines in Figures B.1 and B.2 of the Supporting Information as strong adsorption onto the silica surface. Equilibrium is established within a few minutes. Desorption is also fast and almost complete, signifying reversible adsorption. The frequency shift is −14.4 ± 1.4 Hz for CTAB, corresponding to an adsorption from eq 3 of 9.0 ± 1.0 μmol/m^2. This result agrees with the 9.5 ± 0.4 μmol/m^2 adsorption reported by Macakova et al. (49) For $C_{10}E_4$, the adsorption is 10.2 ± 0.4 μmol/m^2 according to a frequency change of −19.3 ± 0.7 Hz in general agreement with the reflectometry data of Theodoly et al.(51) for aqueous $C_{12}E_5$ at the cmc. These results reinforce successful use of QCMD to detect adsorption kinetics for strongly adsorbing aqueous solutes.

3.2. QCMD of Aqueous Carboxylates

Figure 4 displays measured results (solid lines) for four loading/washout histories of sodium benzoate (0.08 M) and calcium chloride (0.1 M) salt solutions and their combination. The loading/elution sequence is NaBen, $CaCl_2$, NaBen plus $CaCl_2$, NaBen, and $CaCl_2$. Frequency changes (black) are negative, and dissipation shifts (red) are positive, as expected from theory. On the time scale of minutes, loading and washout kinetics are abrupt. The NaBen loading/washout history mimics those of the CTAB and $C_{10}E_4$ surfactants reported in Appendix B of the Supporting Information. It is, thus, tempting to report the frequency shift in Figure 4 as a Sauerbrey adsorption of NaBen. However, in comparison to the surfactant results in Appendix B of the Supporting Information, positive dissipation is now observed, possibly as a result of the increased NaBen concentration compared to those of the surfactants (i.e., 0.08 M in Figure 4 versus 10^{-3} M for the surfactants). Apparently, the product of viscosity and density of the overlying solution contributes to the measured QCMD signals.

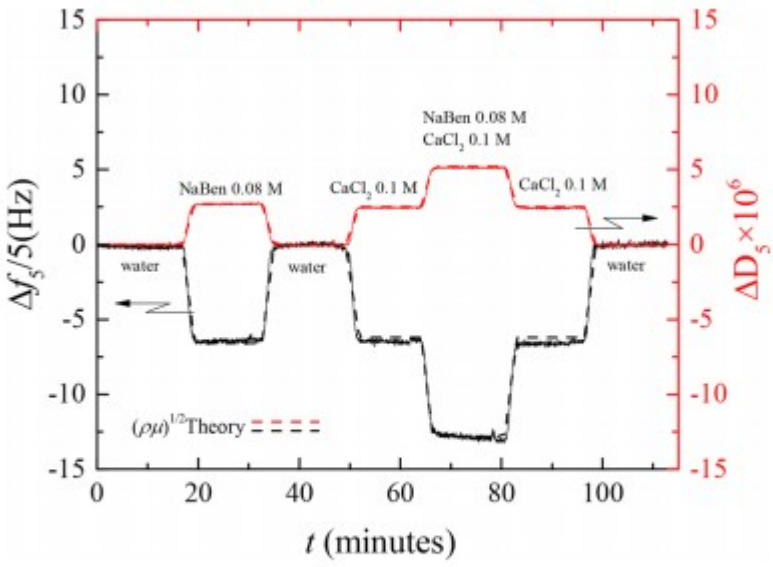

Figure 4. Frequency and dissipation kinetics of 0.08 M sodium benzoate and 0.1 M $CaCl_2$ in four sequential loading and washout experiments.

Subsequent loading/washout of $CaCl_2$ brine gives results consistent with the viscosity hypothesis. The 0.1 M concentration of $CaCl_2$ sufficiently increases the aqueous solution viscosity compared to that of pure water to influence both frequency and dissipation. The NaBen plus $CaCl_2$ loading/washout history and those of the final NaBen and $CaCl_2$ elutions are again consistent with a viscosity origin.

To confirm the viscosity hypothesis, dashed lines in Figure 4 for both frequency and dissipation are predicted from eqs 8 and 9 with no adjustable constants. Viscosities and densities are from the literature in Appendix A of the Supporting Information and from eq 10 using the measured dissipation. Essentially, exact agreement arises with zero adsorption. The observed QCMD signals in Figure 4 follow only from the influence of the overlying liquid solution. This conclusion also clearly holds for NaBen and is confirmed separately in Figures A.1 and A.2 of the Supporting Information.

We find that QCMD is precise for liquid adsorption studies when solute adsorption is strong in dilute solution, such that a viscosity–density correction in eq 8 is not important or, equivalently, when

$$\frac{\Gamma}{C\delta\sqrt{\rho\eta} - \sqrt{\rho_l\eta_l}} \gg \quad (11)$$

If eq 11 is not satisfied, QCMD signals must be corrected for the viscosity of the liquid covering. Once corrected, the NaBen results in Figure 4 reveal no detectable adsorption, with or without calcium ions, to within the precision of the instrument.

To test further calcium ion bridging of aqueous carboxylates onto silica, we also studied adsorption of sodium hexanoate and calcium pentanoate. Experimental results of frequency and dissipation of the fifth overtone for all three caboxylates are summarized in the first four columns of Table1 after about 30 min of loading. Columns 5 and 6 in Table1 list the frequency changes after correction for solution viscosity, Δf_{corr}. Two methods of correction are applied: (1) that from eq 8 using literature densities and viscosities (see Table1) and (2) that from eq 10 using measured dissipation. The last two columns in Table1 list the corresponding adsorption densities from the Sauerbrey expression applied to columns 5 and 6 but reported in molar units as Γ (μmol/m^2). Positive-corrected frequency shifts lead to negative adsorption according to the Sauerbrey relation and, therefore, are not physical. In this case, Table1 lists zero adsorption.

Many measured adsorption densities are zero in Table1, while the maximum adsorption density measured is around 2 μmol/m^2 (i.e., instrument precision is ~ ±1 Hz or ~ ±2 μmol/m^2 for the solutes studied). If we adopt the maximum adsorption and an adsorbed area occupancy of about 20 $Å^2$/molecule, we calculate a surface coverage of 20% of a monolayer. Thus, to within the precision of the instrument, we find negligible calcium ion bridging of small carboxylate salts to silica. This conclusion is consistent with the experimental findings obtained independently at KAUST for the same carboxylate salts and concentrations.

By comparison, several authors have reported significantly larger adsorption of aqueous carboxylates on silica. Madsen and Lind(52) found that the maximum adsorption amount of sodium benzoate from aqueous solution on quartz powder was 7.2 μmol/m^2. Spildo et al.(36) measured the adsorption isotherm for sodium benzoate on fumed silica and Aerosil. The maximum adsorption was 5.6 ± 0.6 μmol/m^2 for fumed silica at a concentration higher than 0.04 mol/kg and 7 ± 0.5 μmol/m^2 for Aerosil at a concentration higher than 0.09 mol/kg. Our results for sodium benzoate and also for sodium hexanoate and calcium pentanoate consistently lie below the precision of the Biolin QCMD instrument.

Recently, Wang et al.(30) used QCMD to study the adsorption of sodium hexanoate on silica. Their maximum reported adsorption of NaHex (10 mM) in 20 mM aqueous $CaCl_2$ was about 5.2 μmol/m^2. Wang et al.(30) do not correct for bulk solution density and viscosity. Instead, they use a Voigt viscoelastic layer model for the adsorbed layer because their frequency shifts present overtone-dependent behavior. Unfortunately, a viscous layer permits adsorbed molecules to flow adjacent to the oscillating crystal, which is not possible for attached adsorbate molecules. We repeated one experiment of Wang et al.(30) for 10 mM sodium hexanoate in 20 mM aqueous $CaCl_2$. As described in Appendix C of the Supporting Information, we find that frequency/dissipation kinetics, including overtone dependencies, are well accounted for by changes in solution viscosity with negligible hexanoate adsorption. Overall, our experimental results indicate that calcium

ion bridging of small aqueous carboxylates to anionic silica surfaces is zero or at best weak. Adsorbed amounts are barely measurable to within the precision of the Biolin QCMD equipment.

4. Discussion

Weak calcium bridging on silica was unexpected. To rationalize this observation, we pursued a classical triple-layer model (TLM) of the silica/aqueous brine surface. Specifically, we elucidate the surface chemistries that control calcium ion bridging. TLMs of ionogenic surfaces are legion.(39−41) A schematic of the silica/brine interface is given in Figure 5. Ionogenic models demand a considerable number of parameters, namely, equilibrium constants for the various proposed surface equilibrium reactions, integral capacitances, and surface hydroxyl site densities. The reactions and parameters chosen are in Table D.1. Calibration of the TLM is in comparison to literature surface titration data of Dove and Craven(53) and Kosmulski et al.(54) for silica suspensions in aqueous NaCl and $CaCl_2$ solutions.

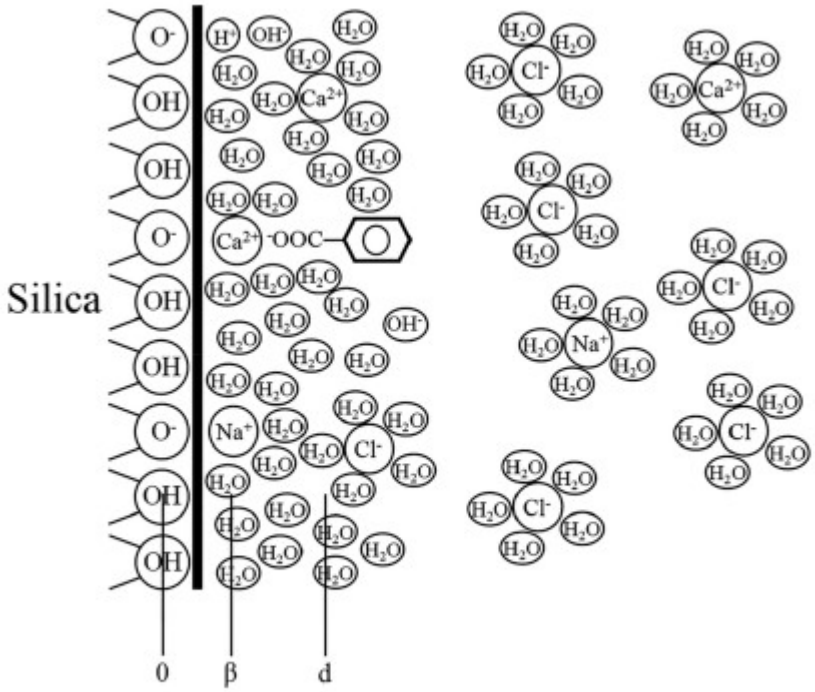

Figure 5. Schematic of TLM ion distributions at the silica/water surface.

Figure 6 shows the surface site densities of silanol, silanate, and calcium silanate as a function of pH in the presence of 0.1 M aqueous calcium chloride. Figure 7 similarly shows the same surface-site densities but now as a function of the $CaCl_2$ concentration at pH 7. Two important findings arise from these figures. First, only a small fraction of the total accepted 5 sites/nm^2 surface density(38,55) of silanol moieties is ionized. Even at pH 9, less than 30% of available ionogenic sites are charged. Second, of the ionized silanate sites, less than half are in the calcium form. This means that

calcium ion binding does not reverse the charge of the silica surface. Relatively high concentrations of calcium ions do not change this picture.

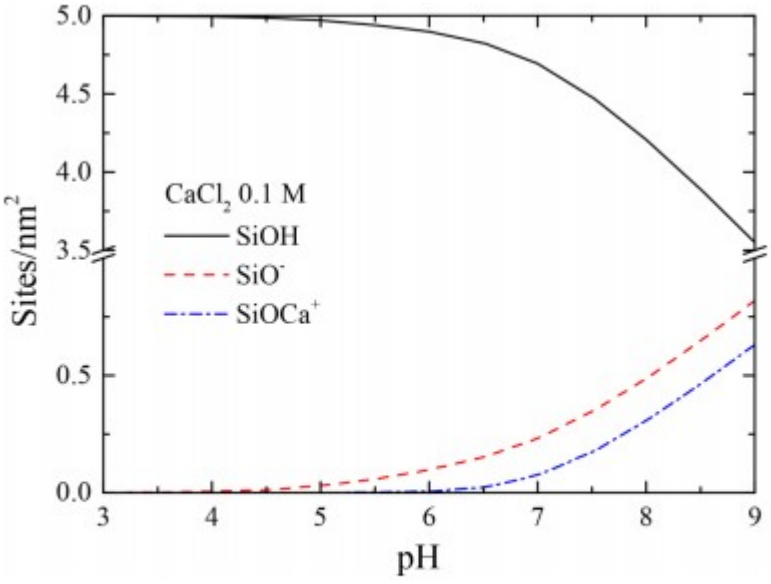

Figure 6. Predicted surface site densities of silica in 0.1 M aqueous $CaCl_2$ as a function of pH according to TLM. Model parameters are listed in Table D.1 of the Supporting Information.

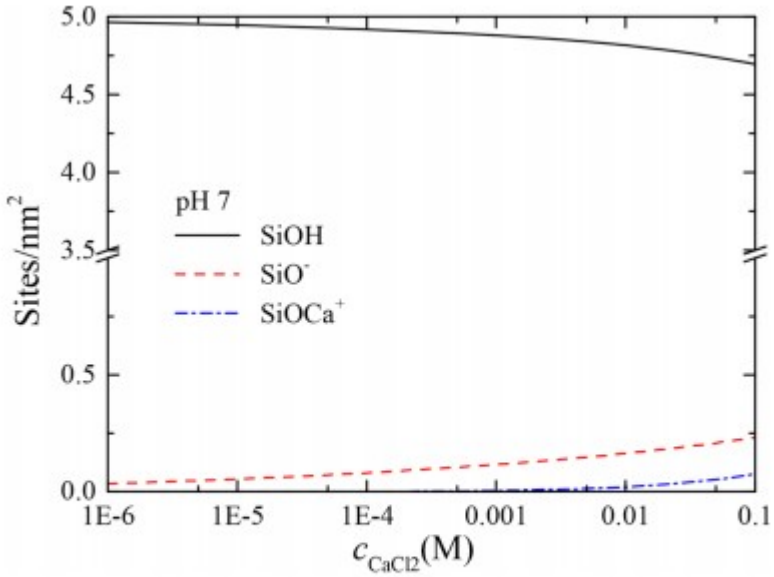

Figure 7. Predicted surface site densities of silica at pH 7 as a function of aqueous $CaCl_2$ according to TLM. Model parameters are listed in Table D.1 of the Supporting Information.

Carboxylate anion adsorption is treated in our TLM as calcium ion bridging to silanate sites according to eq 1. Figure 8 gives the predicted adsorption isotherm in 0.1 M aqueous $CaCl_2$ at pH 7 for two equilibrium constants of 10^3 and 10^4 L/mol. These values are 11–12 orders of magnitude larger than

that for calcium ion binding to the silica surface. Adsorption is weak up to benzoate concentrations approaching the solubility limit. The proposed simple TLM give results consistent with our experimental findings.

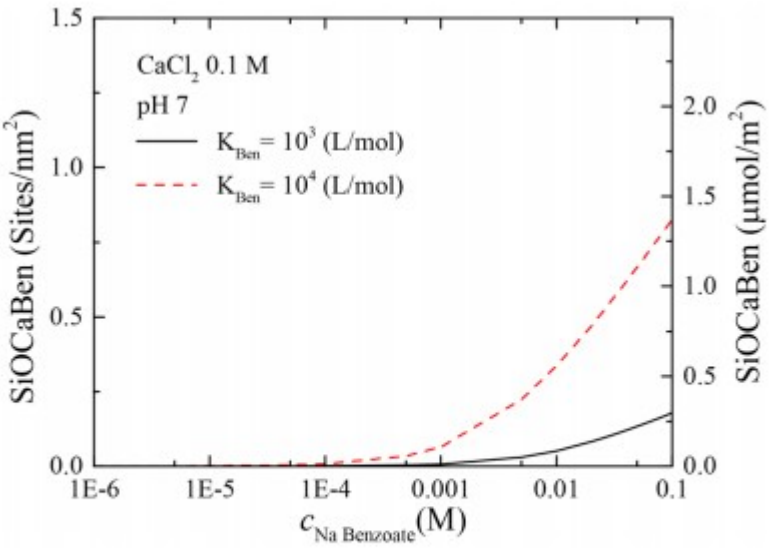

Figure 8. Adsorption of benzoate anion on silica in 0.1 M aqueous $CaCl_2$ at pH 7. TLM parameters are listed in Table D.1 of the Supporting Information.

5. Conclusion

Divalent cation bridging of aqueous anions requires significant ion binding of the divalent ion to a significantly negative-charged surface, likely reversing the surface charge. If the negative surface charges are sufficiently close, however, divalent aqueous cations can ion complex with two adjacent surface sites, giving a neutral-charged surface that does not encourage anionic species bridging. Additionally, the aqueous anion must ion complex strongly to the divalent bridging cation. In the case of calcium ion bridging of small aqueous carboxylates to silica studied here, the TLM reveals insufficient negative charge density of the silica surface in both acidic and alkaline solutions and subsequent insufficient calcium ion complexing. Calcium ion does not reverse the surface charge of silica. TLM predicts minimal carboxylate anion uptake, even when using unrealistic large binding constants. Our QCMD experiments are consistent with the TLM predictions.

The lack of carboxylate calcium ion bridging to silica does not abrogate MIE as a viable recovery mechanism in LSW. Small aqueous-soluble carboxylates may not chemically represent asphaltene carboxylate side groups dangling from the oil/brine interface. Other reservoir mineral surfaces, specifically kaolinite clays in sandstones and calcite in carbonate reservoirs, may provide surface charges that host multivalent cation bridging sites. Also, other binding groups in asphaltene molecules, such as amines, may serve as surface-binding moieties. However, the MIE oil recovery mechanism does demand molecular proximity of the binding moieties to the mineral surfaces.

Thick water layers intervening between crude oil and reservoir rock protect against attachment of asphaltene molecules.

Acknowledgments

Xiaozhen Hu gratefully acknowledges the China Scholarship Council (CSC) and the National Natural Science Foundation of China (51476130) for financial assistance during his stay at the University of California, Berkeley. Saleh Hassan was supported by the Ali I. Al-Naimi Petroleum Research Center (ANPERC) at the King Abdullah University of Science and Technology (KAUST), Thuwal, Kingdom of Saudi Arabia.

References

(1) Yildiz, H. O.; Morrow, N. R. Effect of brine composition on recovery of Moutray crude oil by waterflooding. J. Pet. Sci. Eng. 1996, 14 (3−4), 159−168. (2) Jadhunandan, P. P.; Morrow, N. R. Effect of Wettability on Waterflood Recovery for Crude-Oil/Brine/Rock Systems. SPE Reservoir Eng. 1995, 10 (01), 40−46. (3) Tang, G.-Q.; Morrow, N. R. Influence of brine composition and fines migration on crude oil/brine/rock interactions and oil recovery. J. Pet. Sci. Eng. 1999, 24 (2−4), 99−111. (4) Morrow, N. R. Wettability and Its Effect on Oil Recovery. JPT, J. Pet. Technol. 1990, 42 (12), 1476−1484. (5) Morrow, N. R.; Tang, G.-q.; Valat, M.; Xie, X. Prospects of improved oil recovery related to wettability and brine composition. J. Pet. Sci. Eng. 1998, 20 (3−4), 267−276. (6) Tang, G. Q.; Morrow, N. R. Salinity, Temperature, Oil Composition, and Oil Recovery by Waterflooding. SPE Reservoir Eng. 1997, 12 (04), 269−276. (7) Morrow, N.; Buckley, J. Improved Oil Recovery by Low-Salinity Waterflooding. J. Pet. Technol. 2011, 63 (05), 106−112. (8) Brady, P. V.; Morrow, N. R.; Fogden, A.; Deniz, V.; Loahardjo, N.; Winoto. Electrostatics and the Low Salinity Effect in Sandstone Reservoirs. Energy Fuels 2015, 29 (2), 666−677. (9) Kovscek, A. R.; Wong, H.; Radke, C. J. A pore-level scenario for the development of mixed wettability in oil reservoirs. AIChE J. 1993, 39 (6), 1072−1085. (10) Sheng, J. J. Critical review of low-salinity waterflooding. J. Pet. Sci. Eng. 2014, 120, 216−224. (11) Myint, P. C.; Firoozabadi, A. Thin liquid films in improved oil recovery from low-salinity brine. Curr. Opin. Colloid Interface Sci. 2015, 20 (2), 105−114. (12) Jackson, M. D.; Vinogradov, J.; Hamon, G.; Chamerois, M. Evidence, mechanisms and improved understanding of controlled salinity waterflooding part 1: Sandstones. Fuel 2016, 185, 772−793. (13) Salathiel, R. A. Oil Recovery by Surface Film Drainage In Mixed-Wettability Rocks. J. Pet. Technol. 1973, 25 (10), 1216−1224. (14) Freer, E. M.; Svitova, T.; Radke, C. J. The role of interfacial rheology in reservoir mixed wettability. J. Pet. Sci. Eng. 2003, 39 (1− 2), 137−158. (15) Schmatz, J.; Urai, J. L.; Berg, S.; Ott, H. Nanoscale imaging of pore-scale fluid-fluid-solid contacts in sandstone. Geophys. Res. Lett. 2015, 42 (7), 2189−2195. (16) Buckley, J. S.; Morrow, N. R. Characterization of Crude Oil Wetting Behavior by Adhesion Tests. Proceedings of the SPE/DOE Enhanced Oil Recovery Symposium; Tulsa, OK, April 22−25, 1990; DOI: 10.2118/20263-MS. (17) Buckley, J. S. Evaluation of

Reservoir Wettability and Its Effect on Oil Recovery; Office of Fossil Energy, United States Department of Energy (U.S. DOE): Morgantown, WV, 1999; DE-FC22-96ID13421. (18) Berg, J. C. An Introduction to Interfaces & Colloids: The Bridge to Nanoscience; World Scientific: Singapore, 2010. (19) Mahani, H.; Berg, S.; Ilic, D.; Bartels, W.-B.; Joekar-Niasar, V. Kinetics of Low-Salinity-Flooding Effect. SPE Journal 2015, 20 (01), 008−020. (20) Derkani, M.; Fletcher, A.; Abdallah, W.; Sauerer, B.; Anderson, J.; Zhang, Z. Low Salinity Waterflooding in Carbonate Reservoirs: Review of Interfacial Mechanisms. Colloids and Interfaces 2018, 2 (2), 20. (21) Yutkin, M. P.; Mishra, H.; Patzek, T. W.; Lee, J. Y.; Radke, C. J. Bulk and Surface Aqueous Speciation of Calcite: Implications for Low-Salinity Waterflooding of Carbonate Reservoirs. SPE J. 2018, 23 (1), 84−101. (22) Lager, A.; Webb, K. J.; Black, C. J. J.; Singleton, M.; Sorbie, K. S. Low Salinity Oil Recovery∂An Experimental Investigation. Petrophysics 2008, 49 (1), 28−35. (23) Buckley, J. S.; Takamura, K.; Morrow, N. R. Influence of Electrical Surface Charges on the Wetting Properties of Crude Oils. SPE Reservoir Eng. 1989, 4 (03), 332−340. (24) Sjöblom, J.; Simon, S.; Xu, Z. Model molecules mimicking asphaltenes. Adv. Colloid Interface Sci. 2015, 218, 1−16. (25) Adams, J. J. Asphaltene Adsorption, a Literature Review. Energy Fuels 2014, 28 (5), 2831−2856. (26) Aksulu, H.; Hamso, D.; Strand, S.; Puntervold, T.; Austad, T. Evaluation of Low-Salinity Enhanced Oil Recovery Effects in Sandstone: Effects of the Temperature and pH Gradient. Energy Fuels 2012, 26 (6), 3497−3503. (27) Zachara, J. M.; Ainsworth, C. C.; Cowan, C. E.; Thomas, B. L. Sorption of Binary-Mixtures of Aromatic Nitrogen HeterocyclicCompounds on Subsurface Materials. Environ. Sci. Technol. 1987, 21 (4), 397−402. (28) Buckley, J. S.; Liu, Y. Some mechanisms of crude oil/brine/ solid interactions. J. Pet. Sci. Eng. 1998, 20 (34), 155−160. (29) Sutton, R.; Sposito, G. Molecular simulation of humic substance−Ca-montmorillonite complexes. Geochim. Cosmochim. Acta 2006, 70 (14), 3566−3581. (30) Wang, L.; Siretanu, I.; Duits, M. H. G.; Stuart, M. A. C.; Mugele, F. Ion effects in the adsorption of carboxylate on oxide surfaces, studied with quartz crystal microbalance. Colloids Surf., A 2016, 494, 30−38. (31) Wang, X.; Lee, S. Y.; Miller, K.; Welbourn, R.; Stocker, I.; Clarke, S.; Casford, M.; Gutfreund, P.; Skoda, M. W. A. Cation Bridging Studied by Specular Neutron Reflection. Langmuir 2013, 29 (18), 5520−5527. (32) Sposito, G. The Chemistry of Soils, 3rd ed.; Oxford University Press: New York, 2016. (33) Kumar, N.; Wang, L.; Siretanu, I.; Duits, M.; Mugele, F. Salt Dependent Stability of Stearic Acid Langmuir−Blodgett Films Exposed to Aqueous Electrolytes. Langmuir 2013, 29 (17), 5150− 5159. (34) Haagh, M. E. J.; Siretanu, I.; Duits, M. H. G.; Mugele, F. Salinity-Dependent Contact Angle Alteration in Oil/Brine/Silicate Systems: The Critical Role of Divalent Cations. Langmuir 2017, 33 (14), 3349−3357. (35) Gerold, C. T.; Henry, C. S. Observation of Dynamic Surfactant Adsorption Facilitated by Divalent Cation Bridging. Langmuir 2018, 34 (4), 1550−1556. (36) Spildo, K.; Høiland, H.; Olsen, M. K. Adsorption of Benzoic and 4-Heptylbenzoic Acid on Different Silica Substrates from Organic and Aqueous Solution. J. Colloid Interface Sci. 2000, 221 (1), 124− 132. (37) Zaman, A. A.; Tsuchiya, R.; Moudgil, B. M.

Adsorption of a Low-Molecular-Weight Polyacrylic Acid on Silica, Alumina, and Kaolin. J. Colloid Interface Sci. 2002, 256 (1), 73−78. (38) Rimola, A.; Costa, D.; Sodupe, M.; Lambert, J.-F.; Ugliengo, P. Silica Surface Features and Their Role in the Adsorption of Biomolecules: Computational Modeling and Experiments. Chem. Rev. 2013, 113 (6), 4216−4313. (39) Davis, J. A.; James, R. O.; Leckie, J. O. Surface ionization and complexation at the oxide/water interface: I. Computation of electrical double layer properties in simple electrolytes. J. Colloid Interface Sci. 1978, 63 (3), 480−499. (40) Yates, D. E.; Levine, S.; Healy, T. W. Site-binding model of the electrical double layer at the oxide/water interface. J. Chem. Soc., Faraday Trans. 1 1974, 70 (0), 1807−1818. (41) Hunter, R. J. Zeta Potential in Colloid Science: Principles and Applications; Academic Press: San Diego, CA, 1981. (42) Maurer, S. A.; Bedbrook, C. N.; Radke, C. J. Competitive Sorption Kinetics of Inhibited Endo- and Exoglucanases on a Model Cellulose Substrate. Langmuir 2012, 28 (41), 14598−14608. (43) Sauerbrey, G. Verwendung von Schwingquarzen zur Wagung¨ dünner Schichten und zur Mikrowagung.¨ Eur. Phys. J. A 1959, 155 (2), 206−222. (44) Rodahl, M.; Kasemo, B. On the measurement of thin liquid overlayers with the quartz-crystal microbalance. Sens. Actuators, A 1996, 54 (1), 448−456. (45) Kanazawa, K. K.; Gordon, J. G. The oscillation frequency of a quartz resonator in contact with liquid. Anal. Chim. Acta 1985, 175, 99−105. (46) Voinova, M. V.; Rodahl, M.; Jonson, M.; Kasemo, B. Viscoelastic acoustic response of layered polymer films at fluid-solid interfaces: Continuum mechanics approach. Phys. Scr. 1999, 59 (5), 391−396. (47) Saluja, A.; Kalonia, D. S. Measurement of fluid viscosity at microliter volumes using quartz impedance analysis. AAPS PharmSciTech 2004, 5 (3), 68−81. (48) Kurosawa, S.; Tawara, E.; Kamo, N.; Kobatake, Y. Oscillating frequency of piezoelectric quartz crystal in solutions. Anal. Chim. Acta 1990, 230, 41−49. (49) Macakova, L.; Blomberg, E.; Claesson, P. M. Effect of Adsorbed Layer Surface Roughness on the QCM-D Response: Focus on Trapped Water. Langmuir 2007, 23 (24), 12436−12444. (50) Rojas, O. J.; Stubenrauch, C.; Schulze-Schlarmann, J.; Claesson, P. M. Interactions between Nonpolar Surfaces Coated with the Nonionic Surfactantn-Dodecyl-β-d-maltoside. Langmuir 2005, 21 (25), 11836−11843. (51) Theodoly, O.; Cascao-Pereira, L.; Bergeron, V.; Radke, C. J. A˜ Combined Streaming-Potential Optical Reflectometer for Studying Adsorption at the Water/Solid Surface. Langmuir 2005, 21 (22), 10127−10139. (52) Madsen, L.; Ida, L. Adsorption of Carboxylic Acids on Reservoir Minerals From Organic and Aqueous Phase. SPE Reservoir Eval. Eng. 1998, 1 (1), 47−51. (53) Dove, P. M.; Craven, C. M. Surface charge density on silica in alkali and alkaline earth chloride electrolyte solutions. Geochim. Cosmochim. Acta 2005, 69 (21), 4963−4970. (54) Kosmulski, M.; Hartikainen, J.; Maczka, E.; Janusz, W. A. A.; Rosenholm, J. B. Multiinstrument Study of the Electrophoretic Mobility of Fumed Silica. Anal. Chem. 2002, 74 (1), 253−256. (55) Zhuravlev, L. T. The surface chemistry of amorphous silica. Zhuravlev model. Colloids Surf., A 2000, 173 (1−3), 1−38.